Polymer 59 (2015) 226–233

Contents lists available at ScienceDirect

Polymer

journal homepage: www.elsevier.com/locate/polymer

Gelation and cross-link inhomogeneity of phenolic resins studied by small- and wide-angle X-ray scattering and ^{1}H-pulse NMR spectroscopy

Atsushi Izumi [a, *], Toshio Nakao [b], Mitsuhiro Shibayama [b, *]

[a] Corporate R&D Center, Sumitomo Bakelite Co., Ltd., 1-1-5 Murotani, Nishi-ku, Kobe, Hyogo 651-2241, Japan
[b] Neutron Science Laboratory, Institute for Solid State Physics, The University of Tokyo, 5-1-5 Kashiwanoha, Kashiwa, Chiba 277-8581, Japan

ARTICLE INFO

Article history:
Received 5 November 2014
Received in revised form
7 January 2015
Accepted 10 January 2015
Available online 15 January 2015

Keywords:
Phenolic resins
Gelation mechanism
Cross-link inhomogeneity

ABSTRACT

The gelation mechanism and cross-link inhomogeneity of phenolic resins prepared via polycondensation of phenol and formaldehyde under acidic conditions were studied using small- and wide-angle X-ray scattering and ^{1}H-pulse nuclear magnetic resonance spectroscopy. The solvent-swelling technique was applied for both measurements at the initial stage of gelation to enhance the local fluctuations of the cross-link density. The change in the static and dynamic structures obtained through observations of the X-ray scattering functions and the spin–spin relaxation functions, respectively, during the polycondensation reaction indicates the presence of two different mechanisms for the formation and growth of the inhomogeneity that depend on the amount of cross-linker. (i) When there is a stoichiometrically insufficient amount of the cross-linker, inhomogeneous domains with a loosely cross-linked network appear at the initial stage of gelation. The intradomain reactions become dominant in the growth of the inhomogeneous domain and the degree of cross-linking in the domain increases by bridging two unreacted sites in the network structure via the cross-linker. (ii) When there is a stoichiometric amount of the cross-linker, inhomogeneous domains with a tightly cross-linked network appear at the initial stage of gelation. The interdomain reactions become dominant in the growth of the domain and the size of the domain increases by incorporating new polymer chains into the domain via the cross-linker.

1. Introduction

Phenolic resins were the first artificial plastics developed that were based on a synthetic polymer, and were invented by Baekeland in 1907. Because of their excellent mechanical properties as well as heat and solvent resistance, they have been employed as insoluble and infusible thermosetting resins in electronics, automotive, housing, and other industries [1]. The basic chemical structure of phenolic resins comprises a three-dimensional cross-linked network of three functional phenols and two functional methylenes. Three methylenes can connect to a phenol, one at the *para*-position and the other two at the two *ortho*-positions that are adjacent to the hydroxyl group of the phenolic ring. This cross-linked network provides the abovementioned desirable properties and it is believed that the inhomogeneity of the cross-linked structure influences these properties. However, structural analysis of phenolic resins is difficult because of their insolubility in common organic solvents and their infusibility. Therefore, elucidation of their cross-linked structure and inhomogeneity has been one of the major challenging objectives of the structural analysis of phenolic and other thermosetting resins. The definition of "inhomogeneity of thermosetting resins" is well summarized in the literature [2,3].

It is well known that the case of the inhomogeneity of phenolic resins was first raised by de Boer and Houwink in 1936 [4,5]. As described in our previous paper [6], arguments regarding the inhomogeneity of phenolic and other thermosetting resins, and their structure–property relationships persist even today through observations using scanning and transmission electron microscopy [7–13], atomic force microscopy [12,14,15], small- and wide-angle X-ray scattering (SAXS and WAXS, respectively), and small-angle neutron scattering (SANS) [2,6,16–21].

* Corresponding authors.
E-mail addresses: atsushi_i@sumibe.co.jp (A. Izumi), sibayama@issp.u-tokyo.ac.jp (M. Shibayama).

http://dx.doi.org/10.1016/j.polymer.2015.01.018
0032-3861/

Of these methods, SANS and SAXS have proven to be powerful techniques for elucidating the cross-link inhomogeneity of gel networks [22–28]. In most cases, these scattering methods utilize the swelling feature of the gel; swelling enhances the local fluctuations of the cross-link density because the degree of swelling depends on the degree of cross-linking. The enhancement of the spatial inhomogeneity of the gel network results in a large scattering contrast. However, it is difficult to apply this solvent-swelling technique to highly cross-linked thermosetting resins and only a few studies have addressed cross-link inhomogeneity in phenolic and other thermosetting resins using these scattering methods as compared to the number of SEM and TEM studies of inhomogeneity. ^{1}H-pulse nuclear magnetic resonance (NMR) spectroscopy is also one of the most promising techniques for elucidating the cross-link inhomogeneity of gel networks [29–35]. ^{1}H-pulse NMR spectroscopy offers the spin–spin relaxation time of protons, which is related to the mobility of molecules to which the protons are attached; the lower the molecular mobility, the shorter the relaxation time. For cross-linked polymers, the molecular mobility of polymer segments strongly depends on their local cross-link density [36] and the spin–spin relaxation of tightly cross-linked segments with lower molecular mobility decays faster than that of loosely cross-linked segments.

For theoretical understanding of the cross-linked network structure and the structure–property relationships of phenolic and other thermosetting resins, computer simulations, such as statistical and kinetic methods, molecular dynamics (MD) simulations, and Monte Carlo (MC) simulations, are also promising tools because they are not limited by polymer solubility and infusibility, which always cause experimental difficulties in structural analyses [37–44]. Yamagishi et al. investigated the gelation mechanism of phenolic resins using MC simulations with the cubic percolation theory [41]. According to the simulation results for a polycondensation system with an initial formaldehyde-to-phenol molar ratio of 1.2, the intramolecular reaction occurred more frequently in the gel cluster with increasing gel fraction beyond the gel point and resulted in network formation inside the gel. Unfortunately, this significant result for the gelation mechanism of phenolic resins has not yet been precisely evaluated experimentally except for our previous SAXS study [6].

We have been focusing on understanding the inhomogeneity and structure–property relationships of phenolic resins using scattering methods and MD simulations [6,20,21,44,45]. Through these investigations, we concluded that the characterization of the formation and growth mechanisms of gel networks could be important for elucidating the inhomogeneity of fully cured phenolic and other thermosetting resins, because the cross-link inhomogeneity has not been observed for the cured phenolic resins prepared with different amounts of the cross-linking agent by either SANS, SAXS, or SEM studies. In our previous study [6], the gelation mechanisms of phenolic resins have been investigated through solid-state ^{13}C NMR, SAXS, and reaction kinetics including the successful application of this solvent-swelling technique in SAXS analysis at the initial stage of gelation. This provided new gelation mechanisms for the formation and growth of the cross-link inhomogeneity that depend on the amount of cross-linker: (i) when there is a stoichiometrically insufficient amount of the cross-linker, inhomogeneous domains with a loosely cross-linked network appear at the initial stage of gelation and the degree of cross-linking in the domain increases with the reaction time. On the other hand, (ii) when there is a stoichiometric amount of the cross-linker, inhomogeneous domains with a tightly cross-linked network appear at the initial stage of gelation, followed by an increase in the size of the domain. This result of our previous study agrees well with Yamagishi's simulation result; however, additional experimental verification is required to confirm and refine the gelation mechanism.

In this study, we have further investigated the gelation mechanisms of phenolic resins using SAXS, WAXS, and ^{1}H-pulse NMR spectroscopy. The solvent-swelling technique was applied at the initial stage of gelation for all measurements to enhance the local fluctuations of the cross-link density.

2. Experimental

2.1. Materials

Phenol, 37 wt% formaldehyde aqueous solution, anhydrous oxalic acid, tetrahydrofuran (THF), and THF-d_8 with a 99.5% degree of deuteration were purchased from Wako Pure Chemical Industries, Ltd. (Japan). All materials were used without further purification.

Novolac-type phenolic resins **NV12** and **NV15** were prepared via the polycondensation of phenol and formaldehyde with oxalic acid as an acid catalyst, as shown in Fig. 1. The initial molar ratios of phenol/formaldehyde/oxalic acid were 1.0/1.2/0.010 for **NV12** and 1.0/1.5/0.010 for **NV15**. Note that the reaction was performed in a tightly-sealed vial to avoid any slight change in the molar ratio caused by volatilization of the monomers. The initial formaldehyde-to-phenol molar ratios of **NV12** and **NV15** corresponded to off-stoichiometric and on-stoichiometric ratios, respectively, which resulted in polycondensation reactions with a stoichiometrically insufficient amount of the cross-linker and a stoichiometric amount of the cross-linker, respectively. The

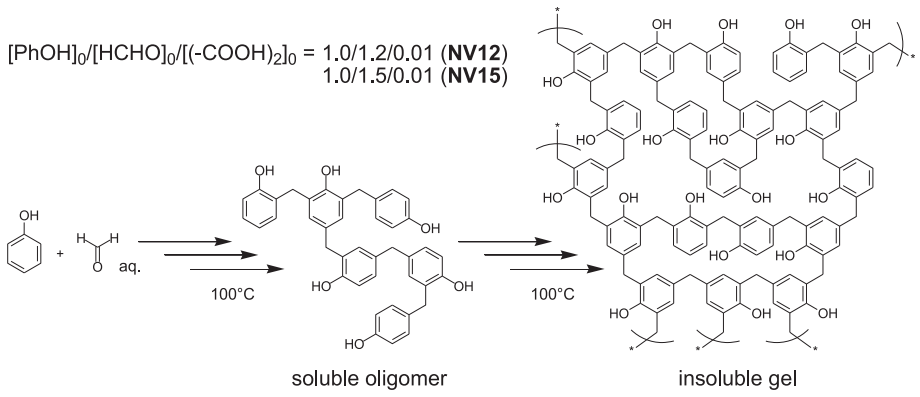

Fig. 1. Polycondensation of phenol and formaldehyde.

reaction was performed at 100 °C for 50, 100, 150, 200, 300, and 450 min; subsequently, the reaction mixtures were milled and washed with water. The gelation occurred at 100 min for **NV12** and 150 min for **NV15**, when a THF-insoluble part was obtained. The details of sample preparation and characterization are described in the literature [6].

2.2. SAXS and WAXS

SAXS experiments over the q range 0.2–7 nm^{-1} were performed on the BL03XU beamline (Frontier Softmaterial Beamline (FSBL)) at SPring-8 that is located in Sayo, Hyogo, Japan [46–48]. A monochromated X-ray beam with a wavelength of 1.0 Å was used to irradiate the samples at room temperature, and the scattered X-rays were counted at a sample-to-detector distance of 1.1 m. The scattered X-rays were counted by an R-AXIS VII++ imaging plate detector system (Rigaku Corporation, Japan) with 3000 × 3000 pixel arrays and a pixel size of 0.1 mm $pixel^{-1}$. WAXS experiments over a q range of 5–20 nm^{-1} were performed on the NANO-Viewer (Rigaku Corporation, Japan). An X-ray beam with a wavelength of 1.54 Å of the CuKα spectral line excited at 40 kV and 30 mA was used. The scattered X-rays were counted at a sample-to-detector distance of 76 mm by a Pilatus 100K detector system (DECTRIS Ltd., Switzerland) with 487 × 195 pixel arrays and a pixel size of 0.172 mm $pixel^{-1}$.

Quartz glass capillaries Mark-Tube (Hilgenburg GmbH, Germany) with a diameter of 2 mm and a wall thickness of 0.01 mm were used for the sample cells. After correction for dark current, background scattering, and transmittance, corrected scattering intensity functions were normalized to the absolute intensity scale using a 1-mm-thick glassy carbon plate (glassy carbon Type 2, Alfa Aesar, USA) as a secondary standard, in which the absolute intensity of the glassy carbon plate was previously determined using a glassy carbon that was provided by Jan Ilavsky of the Advanced Photon Source at Argonne National Laboratory, IL, USA [49].

2.3. ^{1}H-pulse NMR

The ^{1}H-pulse NMR experiments were performed using a JEOL-MU25 spectrometer (JEOL Ltd., Japan) with a 10-mm-diameter probe operated at 25 MHz. Glass NMR tubes (JNM-SM-3340004, JEOL RESONANCE Inc., Japan) with a diameter of 10 mm and a wall thickness of 0.6 mm were used for the sample cells. The spin–spin relaxation time was recorded at room temperature using Carr–Purcell–Meiboom–Gill pulse sequences, in which the pulse width, pulse interval (τ), number of ($180^\circ - 2\tau$)-loops, relaxation delay between subsequent scans, and number of scans were set to 2.0 μs, 50 μs, 1000, 2.0 s, and 128, respectively. Specimens were in 8 wt% semidilute THF-d_8 solution for polymers before the gel point and in the fully THF-d_8 swollen gels for polymers after the gel point.

3. Results and discussion

Fig. 2 shows the change in the X-ray scattering curves of **NV12** and **NV15** during the polycondensation reaction; the curves also show solvent scattering. It should be noted that in the previous study, the scattering curves were investigated after subtracting the solvent scattering intensities from the observed signals according to the polymer fraction that is calculated from the degree of swelling of the gel. The reason for the absence of the solvent scattering correction in this study is to improve the accuracy of data analysis for samples after the gel point. This is done by considering the possibility of a slight deviation of the polymer fraction in the X-ray irradiated volume from that calculated from the degree of swelling. This is because the specimens after the gel point were

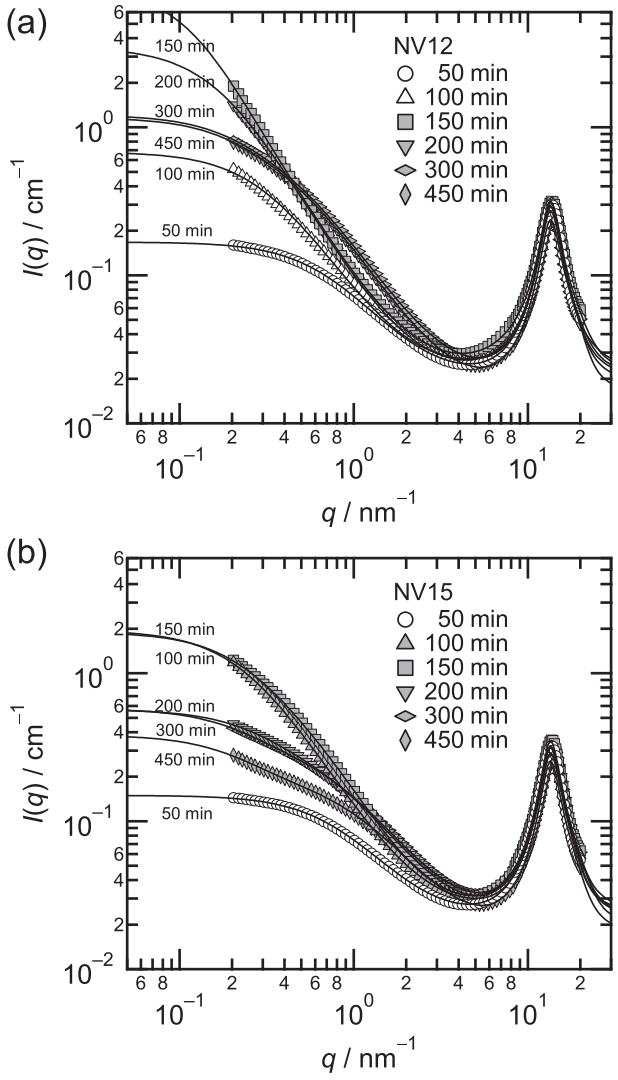

Fig. 2. Change in the X-ray scattering curves: (a) **NV12** and (b) **NV15** in THF. Open and filled symbols represent before and after the gel point, respectively. Solid lines are fitting curves using Equation (2).

deposited as small gel particles in THF, which indicates the existence of a THF region between the gel particles in the X-ray irradiated volume.

According to the previous SAXS study with a q range of 0.2–3 nm^{-1}, the X-ray scattering in this range could result from both the solid-like inhomogeneity and liquid-like fluctuation, which can be explained by the squared Lorentzian equation ($I_{SL}(q)$) [50] and the Ornstein–Zernike equation ($I_{OZ}(q)$) [51], respectively. This combined scattering function has long been used to represent the structure of gels in the swollen state [6,22–28], which is given by

$$I(q) = \frac{I_{SL}(0)}{\left(1 + \Xi^2 q^2\right)^2} + \frac{I_{OZ}(0)}{1 + \xi^2 q^2}, \quad (1)$$

where q, Ξ, and ξ denote the magnitude of the scattering vector, correlation lengths representing the characteristic size of the inhomogeneity and that of the concentration fluctuation, respectively. Here q is given by $q = (4\pi/\lambda)\sin(2\theta/2)$, where λ and 2θ denote the wavelength of the incident beam and the scattering angle, respectively. The first and second terms on the right side

correspond to the solid-like frozen inhomogeneity and the liquid-like fluctuations, respectively. As observed in Fig. 2, all scattering curves have single broad peaks around 4–20 nm^{-1}. These peaks could correspond to short-range electron density fluctuations of both THF and phenolic resins. Thus, the theoretical function of Equation (1) that was used in the previous study is revised to

$$I(q) = \frac{I_{SL}(0)}{\left(1+\Xi^2 q^2\right)^2} + \frac{I_{OZ}(0)}{1+\xi^2 q^2} + A\cdot\exp\left(-\frac{(q-q_0)^2}{2w^2}\right) + B\cdot I_{THF}(q), \tag{2}$$

where A and B, q_0, w, and $I_{THF}(q)$ denote the scaling factors, peak position and width of a Gaussian function that is used to represent the short-range electron density fluctuation of phenolic resins, and observed scattering function of THF, respectively. A curve fitting using Equation (2) is successful for all scattering curves of **NV12** and **NV15**, as shown in Fig. 2 with solid lines.

The change in the fitting parameters during the polycondensation reaction is shown in Fig. 3. The behavior of the change in the parameters agrees well with the results of our previous study with a q range of 0.2–3 nm^{-1}. Here ξ is related to the average size of soluble oligomers and mesh size of the gel network that behaves like a polymer chain in the semidilute regime. Hence, the increase and decrease in the ξ value with reaction time could indicate an increase in the size of soluble polymer chains and a decrease in the mesh size, respectively. The different behavior of the change in the Ξ value between **NV12** and **NV15** could be explained by the difference in their gelation mechanism, which depends on the amount of the cross-linker. When there is a stoichiometrically insufficient amount of the cross-linker, inhomogeneous domains with a loosely cross-linked network appear at the initial stage of gelation. The degree of cross-linking in the domain increases with the reaction time, which results in a decrease in the degree of swelling of the domain. On the other hand, when there is a stoichiometric amount of the cross-linker, inhomogeneous domains with a tightly cross-linked network appear at the initial stage of gelation, followed by an increase in the size of the domain. Thus, a decrease in the Ξ value of **NV12** could be attributed to an increase in the degree of cross-link density in the inhomogeneous domain with a higher cross-link density that results in a decrease in the degree of swelling. In contrast, an increase in the Ξ value of **NV15** could be ascribed to an increase in the size of the domain with a higher cross-link density. This result, with an extended q range of 0.2–20 nm^{-1}, confirms the validity of the gelation mechanism that we have previously proposed.

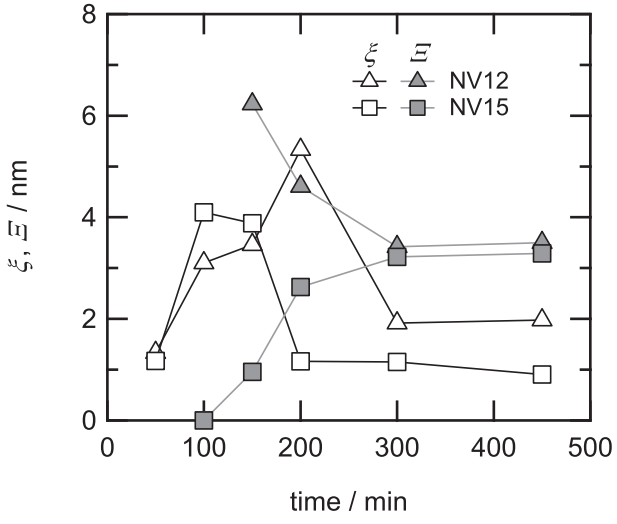

Fig. 3. Change in the fitting parameters. Solid lines are only guides for the eye.

For further verification of the gelation mechanism that is obtained through the analysis of the static structure using X-ray scattering, the dynamics of molecular mobility of the polymer segments are investigated from the viewpoint of a spin–spin relaxation of protons that can be observed using ^{1}H-pulse NMR spectroscopy. Fig. 4 shows the change in the spin–spin relaxation curves of **NV12** and **NV15** during the polycondensation reaction. The polymers are in the THF-d_8 solution state before the gel point and in the fully swollen state in THF-d_8 after the gel point. Here the observed NMR signals could be considered to result only from the spin–spin relaxation of protons in phenolic resins, because a deuterated solvent with a 99.5% degree of deuteration was used for the measurements. Both the relaxation curves of **NV12** and **NV15** decay faster as the reaction proceeds, which indicates a decrease in the average molecular mobility. In general, the spin–spin relaxation function can be described by

$$M(t)/M(0) = \exp\left[-(1/a)(t/T_2)^a\right], \tag{3}$$

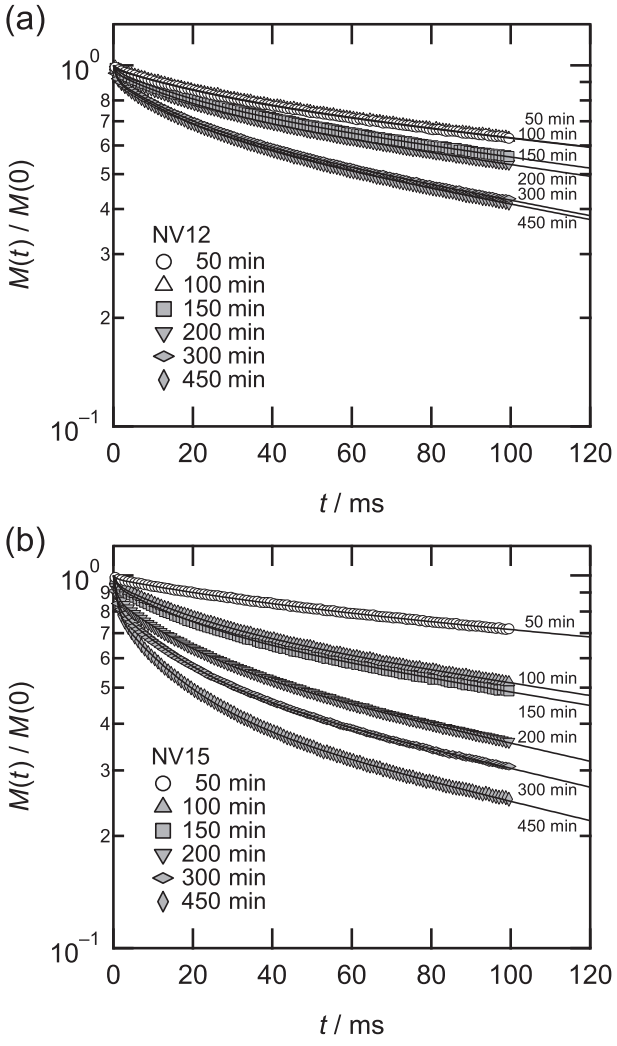

Fig. 4. Spin–spin relaxations of (a) **NV12** and (b) **NV15** in THF-d_8. Open and filled symbols represent before and after the gel point, respectively. Solid lines are fitting curves using Equation (7).

where t, $M(t)/M(0)$, a, and T_2 denote the decay time, normalized magnetization intensity at t, exponent of the decay function, and time constant representing the spin–spin relaxation, respectively [29–31]. The a value ranges from 1 for an exponential-type decay to 2 for a Gaussian-type decay. In polymers with a highly constrained molecular mobility, such as in the glassy and crystalline states, the spin–spin relaxation typically follows the Gaussian-type fast decay. On the other hand, in polymers with a higher molecular mobility, such as in the rubbery and solution states, the spin–spin relaxation follows the exponential-type slow decay. In this study, the a value of 1 could be appropriate because NMR measurements were performed in solvents and polymers are in the solution or swollen states. All the observed relaxation curves, as shown in Fig. 4, cannot be fitted by a single exponential function given by Equation (3) with the a value of 1. This confirms the existence of multiple molecular mobilities of polymer segments in **NV12** and **NV15** that result from the cross-link inhomogeneity, as elucidated by the X-ray scattering analysis. In such a case, a combined function based on Equation (3) should be introduced to explain the spin–spin relaxations of inhomogeneous cross-linked network polymers, which is given by

$$M(t)/M(0) = \sum_{i=1}^{n} \varphi_i \exp\left[-(1/a_i)(t/T_{2,i})^{a_i}\right], \tag{4}$$

where n denotes the number of relaxation modes, and φ_i, a_i, and $T_{2,i}$ represent the molar fraction of protons, a value, and T_2 of the i-th relaxation mode, respectively. Here $\Sigma\varphi_i$ is 1. When the a value is equal to 1, Equation (4) becomes

$$M(t)/M(0) = \sum_{i=1}^{n} \varphi_i \exp(-t/T_{2,i}). \tag{5}$$

At this moment, the n value in Equations (4) and (5) is unknown because no structural model representing the spin–spin relaxation of phenolic resins has been proposed both for solution and swollen states. To evaluate the n value, the following function with a continuous distribution of T_2 given by

$$M(t)/M(0) = \int G(T_2)\exp(-t/T_2)\mathrm{d}T_2 \tag{6}$$

was first considered, where $G(T_2)$ represents a distribution function of T_2. Fig. 5 shows $G(T_2)$ for the relaxation curves shown in Fig. 4, which was calculated using the constrained regularization program CONTIN [52]. CONTIN analysis was performed over the wide range of 10^0–10^4 ms to understand overall features of the distribution function from the narrow range relaxation data. The result clearly indicates that both **NV12** and **NV15** exhibit three different relaxation modes on the order of magnitude 10^0, 10^1, and 10^2–10^3 ms (first, second, and third relaxation modes, respectively) after the gel point, which is irrespective of the polycondensation reaction time. The existence of three relaxation modes confirms the existence of the cross-link inhomogeneity as mentioned above; the cross-linked structure could be classified into three structures with respect to the molecular mobility and the n value should be 3. The first and third relaxation modes would result from the spin–spin relaxations of protons in polymer segments at tightly and loosely cross-linked regions, respectively, and the second relaxation would result from the relaxation at the interface region between the tightly and loosely cross-linked regions. The third relaxation mode would also contain the relaxation of polymer chains in the solution state because the third mode is observed before the gel point at 50 and 100 min for **NV12** and 50 min for **NV15**, where the polymers are soluble in THF-d_8. This relaxation of the sol fraction can be clearly seen as a broadening of $G(T_2)$ to a relaxation time greater than

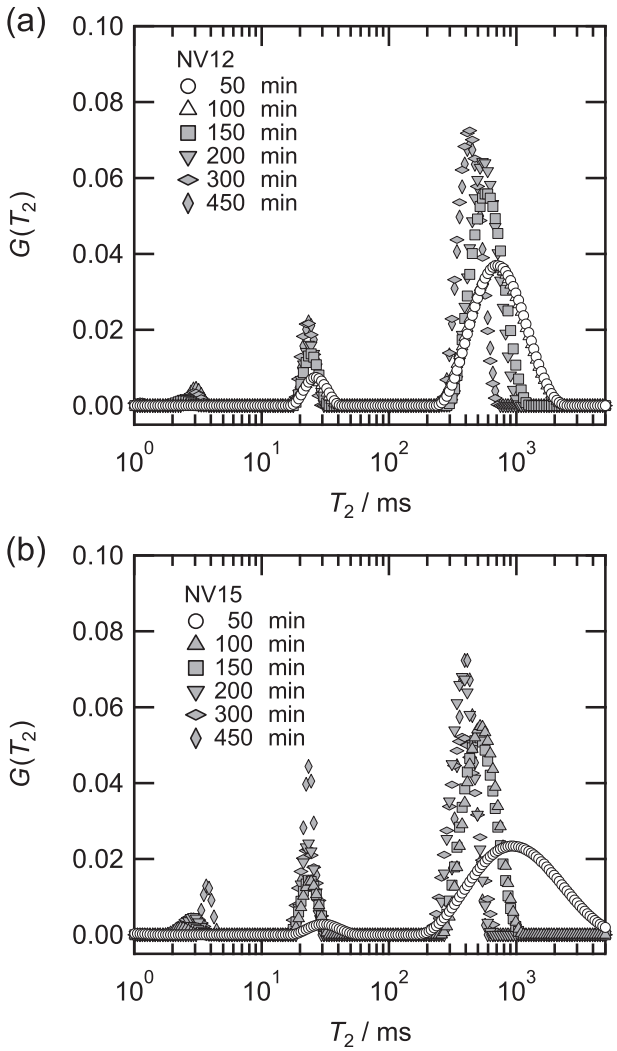

Fig. 5. Spin–spin relaxation time distribution of (a) **NV12** and (b) **NV15**. Open and filled symbols represent before and after the gel point, respectively.

10^3 ms. This result regarding the third relaxation mode indicates that X-ray scattering analysis of the static structure with the Ornstein–Zernike equation cannot distinguish THF-soluble polymer chains from loosely cross-linked polymer segments but ^{1}H-pulse NMR analysis can distinguish them from the viewpoint of the molecular mobility of protons.

To investigate the change in the cross-link inhomogeneity during the polycondensation reaction, the molar fractions of protons in the polymer segments that are assigned to the first, second, and third relaxation modes (φ_1, φ_2, and φ_3, respectively, and $\varphi_1 + \varphi_2 + \varphi_3 = 1$) were evaluated assuming all structures are classified into three structural models with respect to the molecular mobility (*i.e.*, the n value is 3 in Equation (5)). To evaluate the molar fraction, the continuous distribution function as shown in Fig. 5 was reduced to a discrete distribution with three relaxation modes for simplicity. The spin–spin relaxation curves of **NV12** and **NV15** are fitted with a triple exponential function given by

$$\begin{aligned} M(t)/M(0) =& \varphi_1 \exp(-t/T_{2,1}) + \varphi_2 \exp(-t/T_{2,2}) \\ &+ \varphi_3 \exp(-t/T_{2,3}), \end{aligned} \tag{7}$$

where $T_{2,1}$, $T_{2,2}$, and $T_{2,3}$ denote time constants representing the spin–spin relaxation of the first, second, and third modes,

respectively. As shown in Fig. 4 with solid lines, the curve fitting was successful. Moreover, as shown in Fig. 6, these relaxation functions exhibit three different relaxation modes with time constants of 0.5–1 $\times 10^0$, 1–3 $\times 10^1$, and 1–4 $\times 10^2$ ms. These results support the validity of this simplified model using Equation (7).

Fig. 7 shows the change in the φ_{1+2} value obtained as the fitting parameters, where φ_{1+2} denotes the sum of φ_1 and φ_2. This value represents the molar fractions of protons in the polymer segments at the higher cross-link density region where molecular mobility is suppressed by the cross-links and a scattering function of the structure can be expressed by the squared Lorentzian equation. As shown with open symbols in Fig. 7, the φ_{1+2} value is not zero even before the gel point at 50–100 min for **NV12** and at 50 min for **NV15**, which can be attributed to the existence of a second relaxation mode as seen in Fig. 5. This result can be explained by assuming the existence of local loop structures in the THF-soluble fraction. The previous studies on the conformation of phenolic resins before the gel point through an analysis of an exponent of the Mark–Houwink–Sakurada equation demonstrated that the novolac-type phenolic resins prepared by the acid-catalyzed polycondensation reaction contain highly branched structures and have a compact sphere-like conformation in good solvents, such as THF and acetone, compared with a Gaussian chain [21,45,53–58]. Moreover, our previous analysis of the phenol–formaldehyde polycondensation kinetics using a statistical recursive method that was proposed by Aranguren et al. [59] suggested the existence of a loop structure as the reaction reaches the gel point [6]. For further verification of the formation of the loop structure before the gel point, a refinement of the gelation kinetics with a stochastic approach, such as the cascade theory [60,61], would be a promising technique for solving the polycondensation kinetics of phenolic resins more precisely. After the gel point of **NV12** and **NV15**, as shown with filled symbols in Fig. 7, the change in the φ_{1+2} value is clearly different for **NV12** and **NV15**. Initially, **NV12** and **NV15** exhibit similar values—0.20 and 0.25, respectively—immediately after the gel point when they become insoluble in THF. The values of **NV12** and **NV15** increase as the polycondensation reaction proceeds and reach 0.33 and 0.55, respectively. This difference in the slope of the change could result from the difference in the gelation mechanisms of **NV12** and **NV15** and supports the hypothesis that these mechanisms depend on the amount of the cross-linker. (i)

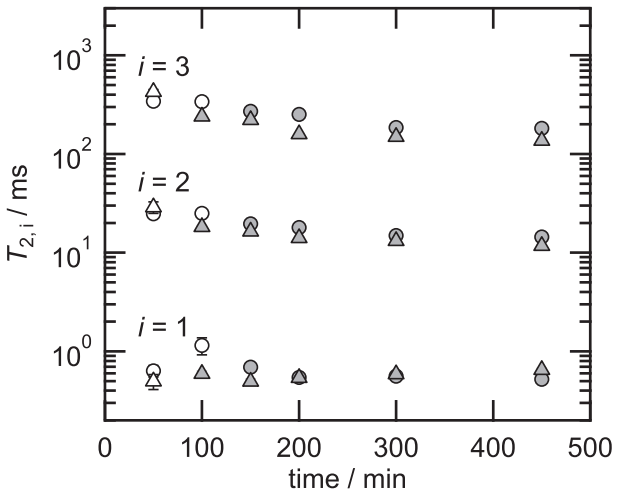

Fig. 6. Change in time constants representing the spin–spin relaxation of the *i*-th relaxation mode: circles, **NV12**; and triangles, **NV15**. Open and filled symbols represent before and after the gel point, respectively.

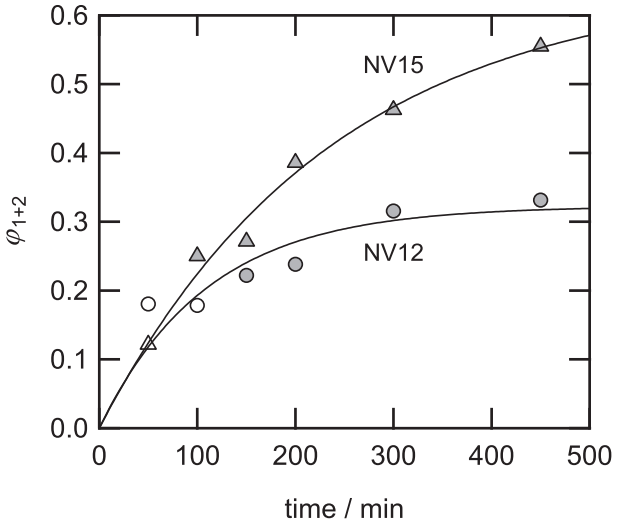

Fig. 7. Change in the molar fraction of protons in the polymer segments at the higher cross-link density region. Open and filled symbols represent before and after the gel point, respectively. Solid lines expressed by single exponential functions are guides for the eye.

When there is a stoichiometrically insufficient amount of the cross-linker at the initial stage of gelation, inhomogeneous domains with a loosely cross-linked network appear and the degree of cross-linking in the domain increases with the reaction time. (ii) When there is a stoichiometric amount of the cross-linker at the initial stage of gelation, inhomogeneous domains with a tightly cross-linked network appear, followed by an increase in the size of the domains with the reaction time. The dominant reaction for the growth of the inhomogeneous domains in these mechanisms should be intradomain reaction in case (i) and interdomain reaction in case (ii), which could result in the difference in the slope of the change in the φ_{1+2} value. In the case of the intradomain reaction, the inhomogeneous domains grow with increase in their degree of cross-linking by bridging two unreacted sites in the network structure via the cross-linker. On the other hand, in case of the interdomain reaction, the inhomogeneous domains grow with increase in their size by incorporating new polymer chains into the domain via the cross-linker. Most of the protons increasing with the growth of the inhomogeneous domain would be characterized as protons of cross-linkers for the intradomain reaction and those of cross-linkers and incorporated polymer chains for which would result in the difference in the slope of the change as seen in Fig. 7. This gelation mechanism of **NV12**, where intradomain reactions enhance the network formation inside the gel, agrees with a simulation result of Yamagishi et al. using Monte Carlo simulations with the cubic percolation theory [41]. This simulation result for a polycondensation system with a $[HCHO]_0/[PhOH]_0$ of 1.2, which is equal to **NV12**, demonstrated that the intradomain reaction in the gel cluster occurred frequently after the gel point. The results of this study clearly show the validity of the abovementioned gelation mechanisms of phenolic resins.

Fig. 8 shows schematic images of the gelation mechanisms representing the dependence of the cross-linker amount on the formation and growth of the inhomogeneity of phenolic resins after the gel point, which was elucidated by SAXS, WAXS, and ^{1}H-pulse NMR study using the solvent-swelling technique at the initial stage of gelation. We believe that the formation of branched phenolic units could play a key role in causing the cross-link inhomogeneity as discussed in our previous paper [6]; namely, the branched units decrease local segmental motion [36], which results in an increase

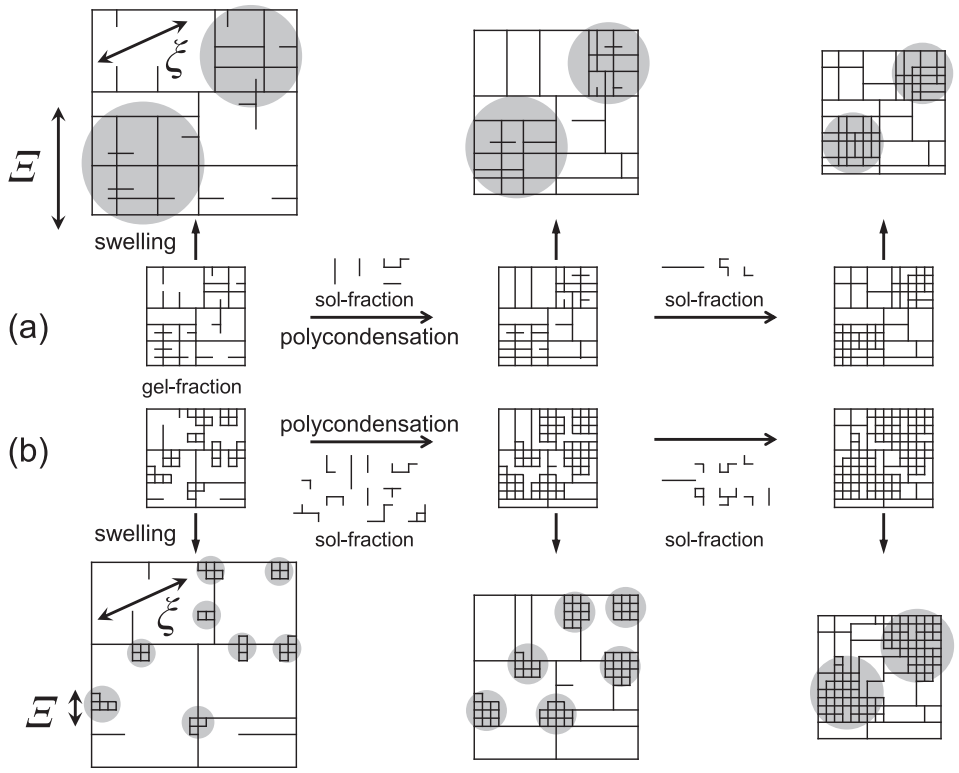

Fig. 8. Schematic image representing the formation and growth of the inhomogeneity during the gelation process of phenolic resins after the gel point with (a) a stoichiometrically insufficient and (b) a stoichiometric amount of the cross-linker, where the dominant reactions are intradomain and interdomain reactions, respectively.

in local fluctuations of the reaction rate and probability of the interdomain and intradomain reactions.

4. Conclusion

The gelation mechanism and cross-link inhomogeneity of phenolic resins prepared via polycondensation of phenol and formaldehyde under acidic conditions were studied using SAXS, WAXS, and ^{1}H-pulse NMR spectroscopy. The solvent-swelling technique was applied at the initial stage of gelation for both measurements to enhance the local fluctuations of the cross-link density. The X-ray scattering curves over the q range of 0.2–20 nm^{-1} are well explained with a combined function of the squared Lorentzian equation, the Ornstein–Zernike equation, a Gaussian function, and a solvent scattering function that represent solid-like cross-link inhomogeneity, liquid-like fluctuation, short-range electron density fluctuation of phenolic resins, and THF scattering from the X-ray irradiated volume, respectively. The spin–spin relaxation curves of protons are well explained with a triple exponential function by assuming a combination of three different molecular mobilities that behave as an exponential function type decay having time constants on the order of magnitude of 10^0, 10^1, and 10^2 ms. After the gel point, these time constants could be attributed to the dynamics of the polymer segments at tightly cross-linked regions, at the interface region between tightly and loosely cross-linked regions, and at loosely cross-linked regions, respectively.

The results of these static and dynamic structure analyses indicate the presence of two different mechanisms for the formation and growth of the inhomogeneity that depend on the amount of the cross-linker. (i) When there is a stoichiometrically insufficient amount of the cross-linker, inhomogeneous domains with a loosely cross-linked network appear at the initial stage of gelation. The intradomain reactions become dominant in the growth of the inhomogeneous domain and the degree of cross-linking in the inhomogeneous domain increases by bridging two unreacted sites in the network structure via the cross-linker. (ii) When there is a stoichiometric amount of the cross-linker, inhomogeneous domains with a tightly cross-linked network appear at the initial stage of gelation. The interdomain reactions become dominant in the growth of the inhomogeneous domain and the size of the inhomogeneous domain increases by incorporating new polymer chains into the domain via the cross-linker.

The gelation mechanism of phenolic resins that we have previously proposed is successfully confirmed and refined by the application of the well-established solvent-swelling technique for structural analysis of gel networks to phenolic resins using a combination of SAXS, WAXS, and ^{1}H-pulse NMR. We believe this structural analysis method offers a new technique for elucidating the inhomogeneity of thermosetting resins.

Acknowledgment

We would like to thank Hitoshi Iwabuki of Industrial Technology Center of Okayama Prefecture for ^{1}H-pulse NMR measurements and helpful discussions. Furthermore, we would like to thank Jan Ilavsky of the Advanced Photon Source at Argonne National Laboratory for providing a glassy carbon plate and its SAXS data on the absolute intensity scale. The SAXS experiments were performed at the second hutch of SPring-8 BL03XU (Frontier Softmaterial Beamline (FSBL)) constructed by the Consortium of Advanced Softmaterial Beamline with the proposal numbers 2013A7201, 2013A7212, 2013A7213, 2013B7251, 2013B7260, and 2013B7261. This study was conducted as a part of the research activities of the Special Interest Group on Thermosetting Resins in the FSBL Consortium comprising the Asahi Kasei research group (Terumasa

Yamasaki, Kimio Imaizumi, Naoki Sakamoto, and Xiaobo Su of Asahi Kasei Corporation, Hisanao Yamamoto of Asahi Kasei E-Materials Corporation, Mitsukazu Ochi of Kansai Univ., and Shinichi Sakurai of Kyoto Institute of Technology), the DENSO research group (Akio Sugiura, Takashi Aoki, and Yasushi Okamoto of DENSO Corporation, Atsushi Takahara of Kyushu Univ., and Sono Sasaki of Kyoto Institute of Technology), and the Sumitomo Bakelite research group (Yasuyuki Shudo, Takuya Hatao, Kazunobu Senoo, and Toshiro Takeda of Sumitomo Bakelite Co., Ltd., and the authors).

References

[1] Gardziella A, Pilato LA, Knop A. Phenolic resins: chemistry, applications, standardization, safety and ecology. 2nd completely rev. ed. Berlin: Springer; 1999.
[2] Dušek K. Angew Makromol Chem 1996;240:1–15.
[3] Pascault JP, Sautereau H, Verdu J, Williams RJJ. Thermosetting polymers. New York: Marcel Dekker; 2002.
[4] de Boer JH. Trans Faraday Soc 1936;32:10–37.
[5] Houwink R. Trans Faraday Soc 1936;32:122–31.
[6] Izumi A, Nakao T, Shibayama M. Soft Matter 2013;9:4188–97.
[7] Spurr RA, Erath EH, Myers H, Pease DC. Ind Eng Chem 1957;49:1839–42.
[8] Erath EH, Spurr RA. J Polym Sci 1959;35:391–9.
[9] Racich JL, Koutsky JA. J Appl Polym Sci 1976;20:2111–29.
[10] Gupta VB, Drzal LT, Adams WW, Omlor R. J Mater Sci 1985;20:3439–52.
[11] Mijović J, Tsay L. Polymer 1981;22:902–6.
[12] Kishi H, Naitou T, Matsuda S, Murakami A, Muraji Y, Nakagawa Y. J Polym Sci Part B: Polym Phys 2007;45:1425–34.
[13] Mijović J, Koutsky JA. Polymer 1979;20:1095–107.
[14] Vanlandingham MR, Eduljee RF, Gillespie JW. J Appl Polym Sci 1999;71:699–712.
[15] Duchet J, Pascault JP. J Polym Sci Part B: Polym Phys 2003;41:2422–32.
[16] Spurr RA, Erath EH, Myers H. Ind Eng Chem 1957;49:1838–9.
[17] Bai SJ. Polymer 1985;26:1053–7.
[18] Dušek K, Pleštil J, Lednický F, Luňák S. Polymer 1978;19:393–7.
[19] Matyi RJ, Uhlmann DR, Koutsky JA. J Polym Sci Part B: Polym Phys 1980;18:1053–63.
[20] Izumi A, Nakao T, Iwase H, Shibayama M. Soft Matter 2012;8:8438–45.
[21] Izumi A, Nakao T, Shibayama M. J Polym Sci Part A: Polym Chem 2011;49:4941–7.
[22] Shibayama M. Macromol Chem Phys 1998;199:1–30.
[23] Shibayama M, Norisuye T. Bull Chem Soc Jpn 2002;75:641–59.
[24] Shibayama M, Karino T, Domon Y, Ito K. J Appl Cryst 2007;40:s43–7.
[25] Shibayama M. Polym J 2011;43:18–34.
[26] Shibayama M. Soft Matter 2012;8:8030–8.
[27] Bastide J, Candau SJ. Structure of gels as investigated by means of static scattering techniques. In: Cohen Addad JP, editor. Physical properties of polymeric gels. New York: John Wiley; 1996. p. 143–308.
[28] Wu WL, Shibayama M, Roy S, Kurokawa H, Coyne LD, Nomura S, et al. Macromolecules 1990;23:2245–51.
[29] Cohen Addad JP. NMR and statistical structures of gels. In: Cohen Addad JP, editor. Physical properties of polymeric gels. New York: John Wiley; 1996. p. 39–86.
[30] Yasunaga H, Kobayashi M, Matsukawa S, Kurotsu H, Ando I. Annu Rep NMR Spectrosc 1997;34:39–104.
[31] Kimmich R, Fatkullin N. Adv Polym Sci 2004;170:1–113.
[32] Fukumori K, Kurauchi T, Kamigaito O. Polymer 1990;31:713–20.
[33] Russel TP, Lee DS, Nishi T, Kim SC. Macromolecules 1993;26:1922–9.
[34] Tanaka H, Fukumori K, Nishi T. J Chem Phys 1998;89:3363–72.
[35] Nomoto M, Fujikawa Y, Komoto T, Yamanobe T. J Mol Struct 2010;976:419–26.
[36] Dušek K. Polym Gels Netw 1996;4:383–404.
[37] Binder K. Monte Carlo and molecular dynamics simulations in polymer science. Oxford: Oxford University Press; 1995.
[38] Kremer K, Müller-Plathe F. Mol Simulat 2002;28:729–50.
[39] Dušek K, Dušková-Smrčková M. Macromol React Eng 2012;6:426–45.
[40] Yang S, Chui Z, Qu J. J Phys Chem B 2014;118:1660–9.
[41] Yamagishi T, Nakatogawa T, Ikuji M, Nakamoto Y, Ishida S. Angew Makromol Chem 1996;240:181–6.
[42] Komarov PV, Chiu YT, Chen SM, Khalatur PG, Reineker P. Macromolecules 2007;40:8104–13.
[43] Varshney V, Patnaik SS, Roy AK, Farmer BL. Macromolecules 2008;41:6837–42.
[44] Izumi A, Nakao T, Shibayama M. Soft Matter 2012;8:5283–92.
[45] Izumi A, Takeuchi T, Nakao T, Shibayama M. Polymer 2011;52:4355–61.
[46] Masunaga H, Ogawa H, Takano T, Sasaki S, Goto S, Tanaka T, et al. Polym J 2011;43:471–7.
[47] Ogawa H, Masunaga H, Sasaki S, Goto S, Tanaka T, Seike T, et al. Polym J 2013;45:109–16.
[48] Takahara A, Takeda T, Kanaya T, Kido N, Sakurai K, Masunaga H, et al. Synchrotron Radiat News 2014;27:19–23.
[49] Zhang F, Ilavsky J, Long GG, Quintana JPG, Allen AJ, Jemian PR. Metall Mater Trans A 2010;41A:1151–8.
[50] Debye P, Bueche AM. J Appl Phys 1949;20:518–25.
[51] Stanley HE. Introduction to phase transitions and critical phenomena. New York: Oxford University Press; 1971.
[52] Provencher SW. Comput Phys Commun 1982;27:213–27.
[53] Ishida S, Nakagawa M, Suda H, Kaneko K. Koubunshi Kagaku 1971;28:250–3.
[54] Tobiason FL, Chandler C, Schwarz FE. Macromolecules 1972;5:321–5.
[55] Kamide K, Miyakawa Y. Makromol Chem 1978;179:359–72.
[56] Sue H, Nakamoto Y, Ishida S. Polym Bull 1989;21:97–104.
[57] Yamagishi T, Kumagai H, Hasegawa T, Nakamoto Y, Ishida S. Polym Int 1995;36:333–8.
[58] Yamagishi T, Nomoto M, Yamashita S, Yamazaki T, Nakamoto Y, Ishida S. Macromol Chem Phys 1998;199:423–8.
[59] Aranguren MI, Borrajo J, Williams RJJ. Ind Eng Chem Prod Res Dev 1984;23:370–4.
[60] Nakao T, Tanaka F, Kohjiya S. Macromolecules 2002;35:5649–56.
[61] Nakao T, Tanaka F, Kohjiya S. Macromolecules 2006;39:6643–52.